American Mineralogist, Volume 83, pages 147–158, 1998

Aqueous Pb sorption by hydroxylapatite: Applications of atomic force microscopy to dissolution, nucleation, and growth studies

STEVEN K. LOWER,[1,*] PATRICIA A. MAURICE,[1] SAMUEL J. TRAINA,[2] AND ERNEST H. CARLSON[1]

[1]Department of Geology, Kent State University, Kent, Ohio 44242, U.S.A.
[2]School of Natural Resources, Ohio State University, Columbus, Ohio 43210, U.S.A.

ABSTRACT

A combination of atomic force microscopy, scanning election microscopy, transmission electron microscopy, energy dispersive spectroscopy, electron diffraction, and X-ray diffraction were used to study reactions of 0.5–500 mg/L aqueous Pb with $Ca_5(PO_4)_3OH$, hydroxylapatite (HAP), at pH 6 and 22 °C. Following 2 h reaction time, concentrations of Pb_{aq} ($[Pb_{aq}]$) decreased from 500 mg/L to <100 mg/L, and from 0.5–100 mg/L to <15 μg/L. This loss of Pb_{aq} from solution (i.e., sorption) resulted partially from simultaneous dissolution of HAP and precipitation of $Pb_5(PO_4)_3OH$, hydroxypyromorphite (HPY), or another solid Pb phase.

The initial saturation state with respect to HPY (defined as the ratio of the ion activity product to equilibrium solubility product) influenced strongly precipitation processes. At a high degree of saturation (initial $[Pb_{aq}] > 100$ mg/L), small nuclei or aggregates of poorly crystalline HPY precipitated homogeneously in solution. At intermediate saturation (initial $[Pb_{aq}]$ ~10–100 mg/L), large, euhedral needles of HPY precipitated homogeneously in solution. At a low degree of saturation (initial $[Pb_{aq}] < 10$ mg/L), a needle-like Pb-containing phase grew heterogeneously on HAP. These results agree well with concepts derived from nucleation and growth theories and demonstrate that initial saturation state influences strongly the sorption process.

INTRODUCTION

Pb is one of the most ubiquitous and hazardous environmental pollutants. As levels of Pb in the environment continue to grow, it is becoming increasingly important to develop methodologies for in-situ remediation of Pb-contaminated sites. The release rate of Pb from different sources depends upon Pb mineralogy, with slow rates of Pb dissolution resulting in decreased Pb bioavailability (Davis et al. 1993). Similarly, the slow rate of dissolution of Pb minerals in an organism's gastrointestinal tract is believed to decrease Pb bioavailability (Davis et al. 1992; Ruby et al. 1992). If these premises are correct, the bioavailability of Pb should be reduced by trapping it in minerals with low solubilities.

Nriagu (1972, 1973a, 1973b) suggested the application of phosphate as an in-situ method to control hazardous quantities of Pb. The relative solubilities of Pb compounds indicate that lead phosphates are more stable under ambient environmental conditions than lead oxides, hydroxides, carbonates, and sulfates (Nriagu 1984; Ruby et al. 1994). Suzuki et al. (1981, 1982, 1984) have shown that $Ca_5(PO_4)_3OH$, hydroxylapatite (HAP), immobilizes aqueous Pb (Pb_{aq}).

Absorption of Pb on the surface of HAP, followed by cation substitution with Ca was suggested as the mechanism on the basis of macroscopic solution data (Suzuki et al. 1984; Takeuchi et al. 1988; Takeuchi and Arai 1990). In contrast, Ma et al. (1993, 1994a, 1994b, 1995) and Xu and Schwartz (1994) proposed that the dissolution of HAP provides phosphate for the subsequent precipitation of $Pb_5(PO_4)_3OH$, hydroxypyromorphite (HPY) from solutions containing Pb_{aq} on the basis of macroscopic data with some direct microscopic, spectroscopic, and diffraction evidence.

Considerable research has focused on metal adsorption to mineral surfaces (e.g., Benjamin and Leckie 1981). As described by Sposito (1986), sorption is the loss of a chemical species from an aqueous solution to a contiguous solid phase. Two of the principle mechanisms of sorption include adsorption, the two-dimensional accumulation of matter at the mineral-water interface; and precipitation, the three-dimensional growth of a solid phase. Precipitation reactions are not understood as well (e.g., Scheidegger and Sparks 1996) but may be initiated through homogeneous or heterogeneous nucleation, may involve coprecipitation, and may include surface precipitation (Sposito 1986). The reaction mechanism cannot be determined using macroscopic data alone (Sposito 1986) but instead must be determined using a combination of macroscopic and surface-sensitive approaches (e.g., Junta and Hochella 1994; O'Day et al. 1994).

* Present address: Department of Geological Sciences, Virginia Polytechnic Institute and State University, Blacksburg, Virginia 24061, U.S.A.

0003–004X/98/0102–0147$05.00

This study combines ex-situ tapping-mode atomic force microscopy (TMAFM), scanning electron microscopy (SEM), transmission electron microscopy (TEM), energy-dispersive spectroscopy (EDS), electron diffraction (ED), and X-ray diffraction (XRD) to characterize the reactants and products involved in Pb_{aq} sorption by HAP at various initial Pb_{aq} concentrations ($[Pb_{aq}]_i$). Our research built upon previous studies by Ma et al. (1993, 1994a), by using the same types of reactants and reaction conditions. These techniques allowed us to differentiate the sorption of Pb_{aq} by homogeneous vs. heterogeneous precipitation; however, we were unable to determine whether Pb_{aq} also adsorbed to the HAP surface. The combined approach allowed comparison of newly developed AFM techniques with more classical SEM and TEM techniques to evaluate ex-situ AFM applications to studies involving environmental particles.

Background

Two competing processes, nucleation and crystal growth, occur during the precipitation or crystallization of a solid phase from solution (Berner 1981). When a nucleus forms in solution an interface is created. This creation of a solid-liquid interface has a positive contribution to the net free energy of crystallization (ΔG_{rxn}) (Drever 1988), given by the following equation:

$$\Delta G_{rxn} = \Delta G_{surf} - \Delta G_{bulk},$$

where ΔG_{surf} is the surface contribution and ΔG_{bulk} is the bulk contribution.

Homogeneous nucleation, which precedes growth, can occur spontaneously in solution when saturation exceeds a critical value (Nielsen 1964). The essential requirement for this type of precipitation is the formation of a stable embryonic aggregate of ions or molecules. Such nuclei form as the result of collisions among ions or molecules in solution, although such collisions do not always yield stable nuclei. As a nucleus grows from solution, it encounters a free energy barrier to further growth. This interfacial free energy (ΔG_{surf}) dominates ΔG_{rxn} until the system reaches a maximum value (Fig. 1a). At this point, the energy released from the formation of bonds in the bulk structure (ΔG_{bulk}) dominates, and growth processes occur spontaneously. Hence the nucleus, which is now considered a crystal, grows by a decrease in the free energy of crystallization (Nielsen 1964; Berner 1981). Nucleation and growth continue until a sufficient quantity of dissolved constituents are removed from solution, thereby relieving the supersaturation of the system. Consequently, the processes of nucleation and growth compete for dissolved components.

The saturation state of a system (defined as the ratio of the ion activity product to the equilibrium solubility product) exerts a strong influence on the competing nucleation and growth processes, as shown schematically in Figure 1a. As the degree of saturation (Ω) is increased, there is a decrease in both the free energy barrier to nucleation (E) and in the size of the stable nucleus (n). The

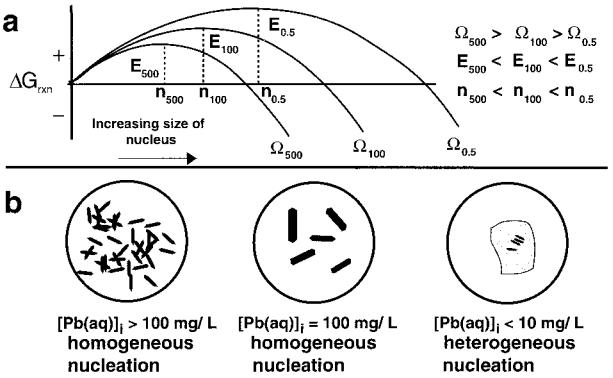

Figure 1. (**a**) Schematic illustration of the role of saturation on the competing processes of nucleation (increasing ΔG_{rxn}) and growth (decreasing ΔG_{rxn}) (modified after Berner 1981). As the degree of saturation is increased, there is a decrease in both the free energy barrier to nucleation and the size of the stable nucleus. (**b**) Predicted morphology of precipitates at various solution saturation states which, for HPY, are strongly dependent upon the initial aqueous Pb concentration ($[Pb_{aq}]_i$). (ΔG_{rxn} = Gibbs energy, Ω = saturation state, E = activation energy, n = size of critical nucleus, subscripts refer to $[Pb_{aq}]_i$ in mg/L).

competition of nucleation and growth processes at different saturation states determines crystal size and morphology (Fig. 1b). At large values of saturation the energy barrier to nucleation is relatively low, and smaller nuclei are stable. Consequently, many small, poorly crystalline nuclei form rapidly in solution thereby consuming most of the dissolved ions, leaving little for growth (Berner 1981). At lesser values of saturation, the energy barrier to nucleation is greater, and large nuclei are stable. Hence, only a few nuclei form in solution and most ions are consumed by growth processes resulting in fewer but larger euhedral crystals, which show high crystallinity (Berner 1981). At extremely small values of saturation, the energy barrier to nucleation and the size required for a stable nucleus are too great. Under such conditions, nuclei form in solution but are unstable and disaggregrate. Hence homogeneous nucleation does not occur. In such cases, nucleation can only take place when the presence of another solid phase reduces the energy barrier to nucleation (Steefel and van Cappellen 1990). This process, called heterogeneous nucleation, is the growth of a solid phase on the surface of another mineral. The suitability of a substrate for heterogeneous nucleation mainly depends on the degree of similarity between the structures of the two phases (Schwertmann and Cornell 1991).

Materials

Hydroxylapatite

We used synthetic HAP from Bio-Rad Laboratories (Hercules, California, U.S.A.), which was grown by treating brushite ($CaHPO_4 \cdot 2H_2O$) with alkali under slow stirring (Tiselius et al. 1956). This material was used as a

FIGURE 2. SEM of hydroxylapatite (HAP) reactant used in batch sorption experiments showing plate-like particles of various sizes (image size = 570 × 410 μm).

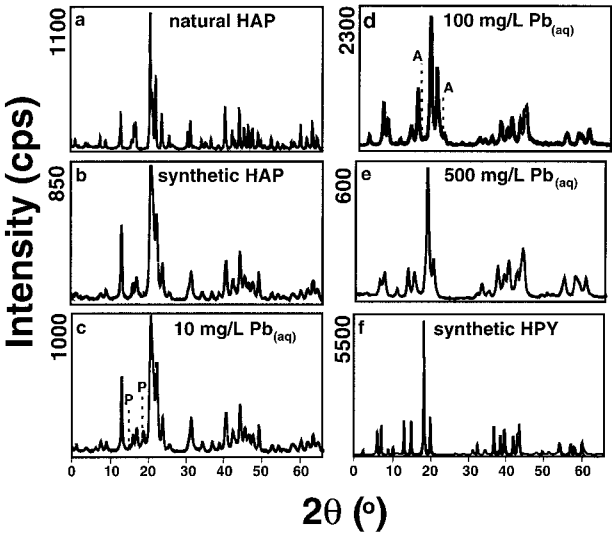

FIGURE 3. X-ray diffractograms of: (**a**) Holly Springs, Georgia HAP; (**b**) synthetic HAP reactant used in this study (reactions of HAP with < 10 mg/L $[Pb_{aq}]_i$ produced similar diffractograms); (**c**) product from reaction of HAP with 10 mg/L $[Pb_{aq}]_i$ (the major hydroxypyromorphite (HPY) peaks are labeled "P"); (**d**) product from reaction of HAP with 100 mg/L $[Pb_{aq}]_i$ (the major HAP peaks are labeled "A"); (**e**) product from reaction of HAP with 500 mg/L $[Pb_{aq}]_i$; and (**f**) synthetic HPY. At $[Pb_{aq}]_i$ 10 mg/L, HPY was detected in the reaction product.

reactant directly as received from the manufacturer, with no grinding or washing procedure.

HAP consists of plate-like crystalline particles <200 μm on edge (Fig. 2). EDS showed only Ca and P. The large difference in refractive indices of HAP and brushite allowed us to determine that no observable residual brushite remained. However the HAP crystals were too small to obtain an optic axis figure with a polarizing microscope. Therefore we are uncertain whether it was monoclinic ($P2_1/b$) (Elliott 1971; Elliott et al. 1973) or hexagonal ($P6_3/m$) (Kay et al. 1964; Hughes et al. 1989, 1990).

Although HAP was the only phase detected by XRD, the peaks were broader and less intense than those produced by natural HAP obtained from a talc-schist in Holly Springs, Georgia (specimen no. R9498 provided by the National Museum of Natural History/Smithsonian Institution) (Figs. 3a and 3b). Because both HAPs were ground to the same size, this may indicate poor crystallinity of the synthetic HAP. The synthetic material was precipitated at temperatures <100 °C and atmospheric pressure (Tiselius et al. 1956), unlike most natural apatite, which forms at much higher temperatures and pressures (Nash 1984). If the synthetic HAP is indeed poorly crystalline, it may react differently than other apatite phases. For example, amorphous materials have been shown to be more reactive than crystalline materials of the same composition (Stumm and Morgan 1981; Parks 1990).

After annealing the HAP at temperatures >800 °C, the XRD pattern showed that an additional phase, whitlockite $[Ca_3(PO_4)_2]$, is present. This result indicates Ca-deficiencies in the HAP structure because Ca-deficient HAP is less stable thermally than stoichiometric HAP, which is not affected by such temperatures (Posner et al. 1984). Such results agree well with analyses of Tiselius et al. (1956), who observed that the Ca to P ratio of a solution in apparent equilibrium with the HAP was less than that expected for stoichiometric HAP, for which Ca/P equals 1.667.

The structural and chemical variations described above are common to most HAPs whether they are synthetic or natural (Posner et al. 1984). Such variations complicate kinetic studies that rely solely on macroscopic observations of solution chemistry.

Hydroxypyromorphite

HPY is known to precipitate when HAP is reacted with solutions of Pb_{aq} (e.g., Ma et al. 1993). Therefore, a specimen of synthetic HPY (sample provided by V. Laperche, Ohio State University) was characterized structurally and chemically. This material was synthesized according to the methods of Narasaraju et al. (1972) by reacting lead nitrate with diammonium hydrogen phosphate at pH 12 and 37 °C. HPY was the only phase detected by XRD (Fig. 3f). Only Pb and P were detected by EDS.

METHODS

Batch experiments

Batch sorption experiments were conducted in high-density polyethylene bottles (Nalgene). Pb solutions were made from $Pb(NO_3)_2$ stock solution (Spex), using Milli-Q H_2O. Reagent grade sodium hydroxide (Fisher Scientific), nitric acid (Aldrich), or both were used to adjust the pH.

Sorption experiments were conducted by reacting 0.1 g of HAP with 200 mL solutions containing 0, 0.5, 1, 10, 100, or 500 mg/L $[Pb_{aq}]_i$. The HAP was added to H_2O and stirred until the solution pH stabilized at an average

value of seven. Pb_{aq} was then added to the system and the pH was immediately adjusted to six. The reaction vessel was covered with aluminum foil and placed on a shaker table at ambient temperature (~22 °C) for 2 h.

Subsequent to reaction, samples were split for various instrumental analyses. Following removal of small volumes of sample for AFM, SEM, and TEM analyses, a portion of the remaining suspension was filtered through 0.1 μm polycarbonate membranes and immediately analyzed for Pb_{aq} and phosphate. The remainder of the solution was centrifuged for XRD analysis.

Each experiment was repeated to assess the reproducibility of the instrumental and chemical techniques. AFM, SEM, TEM, EDS, ED, and XRD analyses were performed on two to four replicates of each experiment. Chemical analyses were performed on three replicates from each experiment.

Atomic force microscopy

We used a Digital Instruments Nanoscope III AFM with a Nikon binocular optical microscope attachment and tapping-mode capability. The principles of AFM as applied to geologic materials have been discussed in detail (e.g., Hochella 1990; Eggleston 1994). Several researchers describe the application of AFM to environmental particles and discuss suggested imaging parameters and identification of artifacts (e.g., Nagy and Blum 1994; Maurice and Lower 1998).

TMAFM imaging of particles requires use of a substrate material. We chose 0.1 μm polycarbonate membranes as substrates. Because detailed measurements of particle dimensions were not conducted, an atomically flat substrate was unnecessary. Because particles much smaller than 0.1 μm in diameter were retained on the membranes, loss of fine particulates is not a concern in imaging.

For TMAFM analysis, small volumes of reacted solution (~0.5–1.0 mL) were syringe filtered onto the membranes. To reduce the potential for precipitation or dissolution upon drying, air was immediately forced from a clean syringe through each membrane, removing the remaining solution from the filter housing. The membranes were then placed sample-side-up on tissues to wick away remaining moisture and quickly transferred to a clean container with a protective cover. Upon drying, the membranes were attached gently to metal AFM stubs using double-sided tape and Parafilm. Observations with the binocular microscope attachment of the AFM insured that the Parafilm did not remove observable amounts of material from the membranes. A comparison with TEM images demonstrated that these preparation techniques were non-destructive.

Samples were imaged in air shortly after preparation because adhesion of particles to the membrane decreases with time. The main benefit of TMAFM for particulate studies is a reduction in lateral frictional forces upon scanning, relative to the commonly used contact mode of imaging (Zhong et al. 1993), thereby reducing the probability of plucking particles off the substrate surface during imaging.

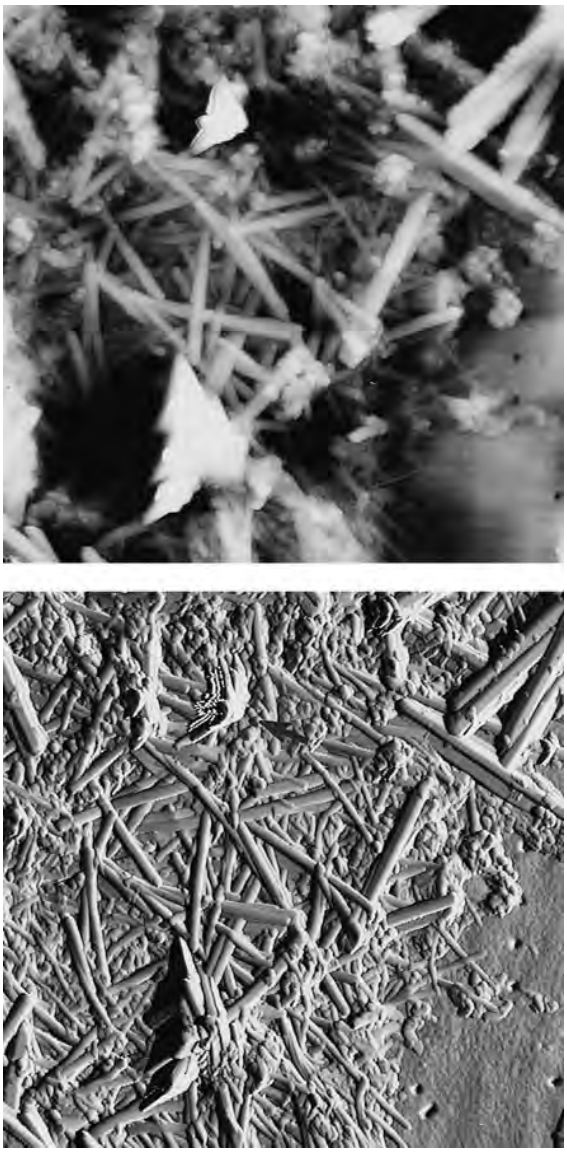

FIGURE 4. HAP reacted with 100 mg/L $[Pb_{aq}]_i$. Comparison of TMAFM height (**top**) and amplitude (**bottom**) images (scan area of each image is 4.50 μm on a side; light areas in height image correspond to high regions, the highest of which is ~400 nm). These images were collected simultaneously and show two distinct particle morphologies: needles and clusters of rounded material. Complementary SEM/EDS, TEM/EDS, and XRD results, indicate the needles are HPY and the rounded clusters are HAP. The height image shows accurate vertical dimensions while the amplitude image provides sharper visual details. Pores in the polycarbonate membrane substrate can be seen in the lower right corner of each image. Tip-sample convolution occurred when the needles were oriented perpendicular to the pc membrane (see arrow).

Relatively sharp etched silicon tips were used to reduce tip-sample convolution (Barrón et al. 1997).

Data were collected simultaneously in the traditional height mode and amplitude mode (Fig. 4). Height images

provide a direct representation of sample microtopography, and are true to scale in *x*, *y*, and *z* directions. Amplitude images display the rate of change in surface microtopography. For very rough surfaces, including the particles imaged here, the amplitude images were perhaps the most important part of the imaging procedure because they provided easily interpretable representations of surfaces that were often much clearer than the height images. However, height (*z*) data are meaningless in amplitude images so that these data could not be used for three-dimensional measurements. With the exception of Figure 4a, all figures presented herein are in amplitude mode. Hence height scales are not presented.

Other microscopy procedures

SEM analysis was conducted on a JEOL 6300-V SEM and a Princeton Gamma Tech ISIABT SEM (model SX-40A) equipped with a microanalyzer EDS. TEM analysis was conducted on a Philips CM200 with a Philips MS EDS and ED capabilities.

After a sample was analyzed by TMAFM, it was coated with carbon or gold and analyzed with SEM and EDS. Samples for TEM analysis were prepared by allowing a few drops of reacted solution to dry on a copper grid. Larger particles did not adhere well to the grid. Hence, TEM analyses may have been biased toward smaller size particles. Each sample was analyzed at numerous locations to provide a representative sampling scheme. By analyzing the same samples with SEM, TEM, and AFM, in some instances we could use EDS capabilities of the other microscopes to help interpret AFM images that lack spectroscopic data.

X-ray diffraction

XRD analysis was performed using an automated Rigaku θ-θ goniometer equipped with a monochromator. All diffraction patterns were obtained using Cu$K\alpha$ radiation at 45 kV and 35 mA. Measurements were made from $2\theta = 3$ to 70° using a scan-speed of 0.5 to 1.0° 2θ per min. Samples were prepared by centrifuging reacted solutions at 2400 rpm for a period of 1 h to concentrate particles >0.1 μm in size (Jackson 1969). The centrifuged solution was decanted and the slurry of concentrated particles was then placed on ceramic tile and allowed to air dry. Side-loaded mounts were prepared to insure a random orientation of grains (Morris et al. 1984). Sometimes there was an insufficient quantity of particles remaining because too many were lost to other preparation techniques. For these samples, a back-loaded mount was prepared (Moore and Reynolds 1989).

Chemical analysis

An inductively coupled plasma emission spectrometer was used to analyze dissolved $[Pb_{aq}] > 500$ μg/L, and an atomic absorption spectrophotometer and graphite furnace was used to analyze dissolved $[Pb_{aq}] < 500$ μg/L. Dissolved phosphate was measured colorimetrically (Murphy and Riley 1962).

TABLE 1. Changes in $[Pb_{aq}]$ upon 2 h reaction with HAP

$[Pb_{aq}]$ initial (mg/L)	$[Pb_{aq}]$ final (μg/L)	
	This work	Ma et al. (1993, 1994a)
500	72 800	89 400
100	6.7	5.6
10	3.2	—
5	—	0.7
1	0.6	—
0.5	0.4	—
0	0.4	1.3

Note: All analyses had a relative standard deviation <5%.

Although the final $[Pb_{aq}]$ was determined for each experiment, phosphate analysis was conducted only on the reaction blank and showed that HAP dissolution did indeed occur within 2 h. Previous studies (e.g., Ma et al. 1993; Xu and Schwartz 1994) of similar Pb-HAP systems concentrated on identifying changes in Pb_{aq}, Ca_{aq}, and phosphate concentrations over time. We chose not to repeat these detailed macroscopic measurements; instead Pb_{aq} and phosphate were analyzed as necessary to check our results against the previous determinations. The precision of all chemical analyses was within 5% relative standard deviation.

RESULTS

Macroscopic measurements

Final $[Pb_{aq}]$ for each experiment (Table 1) agree well with results of Ma et al. (1993, 1994a). These macroscopic observations showed rapid loss of Pb_{aq} by adsorption to the surface of HAP or the precipitation of a solid Pb phase. For example, an $[Pb_{aq}]_i$ of 100 mg/L was reduced to less than 10 μg/L in only 2 h and to ~1 μg/L in 12 h, after which concentration remained approximately constant.

0 mg/L $[Pb_{aq}]_i$

Reaction of HAP with H_2O at pH 6, in the absence of added Pb_{aq} served as a blank. TMAFM of the reaction blank showed clusters or hillocks of material on the surfaces of HAP particles, with no obvious crystallographically controlled dissolution features (Fig. 5). No etch pits were observed at achievable resolution (≥100 nm). The HAP surface did not possess features resembling needles or elongate rods, which were commonly found when HAP was reacted with Pb_{aq}. Nor did SEM and TEM analyses reveal etch pits, instead rounded edges and smaller particle sizes relative to unreacted HAP were seen (Lower 1997). The absence of etch pits and the presence of rounded edges and rounded hillocks on the surface suggests bulk-transport controlled dissolution (Berner 1978). XRD and EDS results were identical to those of unreacted HAP (see Fig. 3b), confirming that the HAP was not converted to another Ca-phosphate phase.

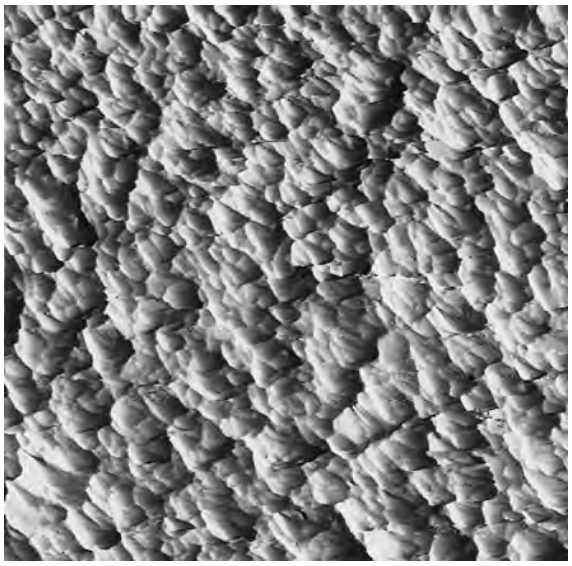

FIGURE 5. HAP reacted with 0 mg/L $[Pb_{aq}]_i$. TMAFM image of the reaction blank showed rounded features with the absence of crystallographically controlled dissolution features (scan area = 2.38 μm on a side). SEM and TEM of the same sample (results not shown) revealed that the HAP particle size decreased and its edges became rounded. XRD results were analogous to the reactant material (see Fig. 3b). EDS (results not shown) were similar to unreacted HAP, showing only Ca and P.

FIGURE 6. HAP reacted with 500 mg/L $[Pb_{aq}]_i$. TMAFM image showing botryoidal masses (see top portion of image) and small intergrown needles (scan area = 2.00 μm on a side). SEM (results not shown) revealed aggregates of morphologically indistinct material. XRD results (see Fig. 3e) indicate that the sample was HPY. EDS (results not shown) indicate that the material imaged with SEM was dominated by Pb and P.

500 mg/L $[Pb_{aq}]_i$

TMAFM imaging of the reaction product showed very small aggregates or nuclei (generally <150 nm in diameter) of morphologically indistinct material (upper region of Fig. 6). A few intergrown, rod-shaped needles were seen (Fig. 6) with roughly micrometer sized lengths and sub-micrometer width.

SEM images of the same samples yielded nondescript, botryoidal masses of material (Lower 1997). SEM was unable to achieve high enough resolution to detect the small needles imaged with AFM, perhaps because of sample coating procedures. Also SEM did not reveal any particles resembling HAP. TEM analysis was not performed on this reaction product.

XRD results showed only HPY present as a reaction product (Fig. 3e). Because HAP was the only source of phosphate, it is likely that the HAP dissolved, producing phosphate that combined with Pb_{aq} to form HPY in solution. The low intensity and broadness of HPY peaks relative to synthetic HPY (Fig. 3f) and HPY produced in other experiments (Figs. 3c and 3d) suggests that a poorly crystalline phase was formed during the reaction. EDS results were similar to those of synthetic HPY and indicate that the mass of material in SEM images was dominated by Pb and P.

100 mg/L $[Pb_{aq}]_i$

TMAFM imaging of the reaction product was extremely difficult because the tip shape interacted with the sample shape (for a discussion of this process, see Griffith and Grigg 1993). With the AFM's binocular microscope attachment, we saw clusters or aggregates of material dispersed across the polycarbonate membrane. Real images could only be collected at the edges of these aggregates (Fig. 4). We suspected that the aggregated masses of reaction products probably consisted of HPY needles oriented largely in a vertical fashion. Hence, the AFM tip shape interacted with the sharp terminations of HPY needles (e.g., see Fig. 4b). Only along the edges of the aggregates of material were the needles lying horizontally. Subsequent SEM analysis of the same sample confirmed this hypothesis.

Tip-sample shape interaction also altered the shapes along the ends of the HPY needles. SEM images showed well-terminated needles; whereas, AFM images showed primarily rounded ends. These results indicate that the needles were composed of hexagonal prism and dipyramidal faces.

As shown in Figure 4, many of the needles imaged with TMAFM were relatively large, generally having a length of ~2 μm. Elongation along the crystallographic *c* axis resulted in a length-to-width ratio of approximately 9:1. These needles were euhedral, showing well-defined crystallographic faces. Some needles were preferentially oriented (Fig. 7a) as opposed to being randomly distributed across the membrane (Fig. 4b).

What we originally assumed was that homogeneous precipitates of a new Pb phase would be randomly distributed, because the solid phase would fall from suspen-

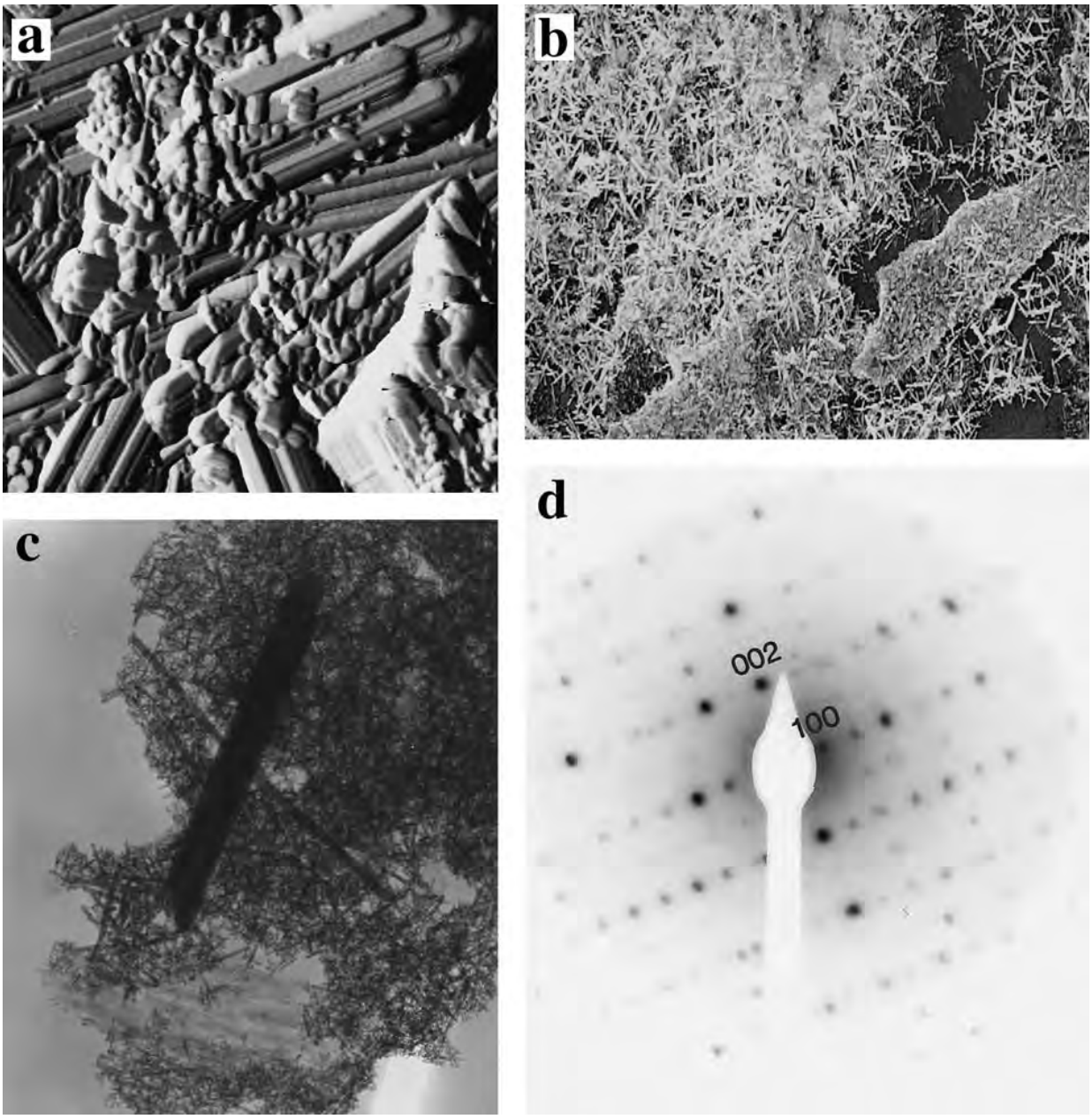

FIGURE 7. HAP reacted with 100 mg/L $[Pb_{aq}]_i$. (**a**) TMAFM image showing numerous needles aligned in the same crystallographic orientations (scan area = 1.84 μm on a side). Such needles are probably parallel intergrowths which formed in solution. (**b**) SEM image showing needles and platelets of material (image size = 50 × 35 μm). The needles are randomly distributed and do not show a preferential association with the platelets. (**c**) TEM image showing very small needles with a few larger needles (image size = 2.70 μm × 3.25 μm). The larger needles are of similar size to those imaged with SEM and TMAFM. (**d**) ED of [010] zone of a needle imaged with TEM. Diffraction spots were smeared, suggesting defects in the crystal lattice. XRD pattern (see Fig. 3d) showed that the sample was dominated by HPY with minor amounts of HAP.

sion onto the membrane (see also Junta and Hochella 1994). Conversely, heterogeneous precipitation would result in preferential alignment of a new phase. At first glance both processes seem to be occurring. However, the aligned needles in Figure 7a appear to be aggregates of identical crystals whose crystallographic axes and faces are parallel. As such, they are more likely parallel intergrowths, which formed in solution as a result of their rapid crystallization (Klein and Hurlbut 1985).

Homogeneous nucleation and growth in solution, rather than heterogeneous nucleation on HAP, is suggested by SEM and TEM pictures of euhedral, doubly terminated

needles that were not preferentially associated with HAP particles (Figs. 7b and 7c). Neither SEM nor TEM detected parallel intergrowths. The needles detected with TEM were smaller than those detected with SEM and AFM but with analogous length-to-width ratios. Combined SEM, AFM, and TEM analyses demonstrated that the needles occurred in a range of sizes.

ED of the needles showed diffraction spots arranged in a crystalline pattern (Fig. 7d). Many of the diffraction spots appeared to be smeared rather than well defined, rounded dots. Although this may result from condensation of the electron beam, the smeared spots more likely indicate that the periodicity of the crystal lattice was disrupted. Structural defects are probably present and consistent with rapid formation of the solid Pb phase.

XRD analysis indicated that the sample was dominated by HPY with minor amounts of HAP (Fig. 3d). EDS indicated that the needles were dominated by Pb and P, and the non-needle material was dominated by Ca and P (Lower 1997). Hence, it seems that most of the Pb_{aq} was bound as HPY needles and that a non-needle morphology in AFM images was indicative of HAP.

10 mg/L $[Pb_{aq}]_i$

Many TMAFM images of the reaction product showed needles similar to those at 100 mg/L $[Pb_{aq}]_i$, however, preferential orientation of some needles was observed. (Fig. 8a). These needles were not identical to those attributed to parallel intergrowths (e.g., Fig. 7a), and seemed to be associated with the surface of another phase. A comparison of these images with those of the reaction blank as well as XRD, SEM-EDS, and TEM-EDS results reinforced the notion that non-needle morphology was indicative of HAP, implicating heterogeneous precipitation of HPY on HAP.

Several intergrowths were imaged with TMAFM (Fig. 8b). Rapid crystallization may have promoted their formation, as intergrowths are energetically less stable than single crystals of the same composition. Although such intergrowths appear to be related by a mirror plane, pyromorphite twins are rare. Hence, we are unsure whether such intergrowths can be classified as twins.

SEM, TEM, EDS, and ED results (Lower 1997) were similar to those for 100 mg/L $[Pb_{aq}]_i$. Neither SEM nor TEM detected the aligned needles found with AFM. XRD revealed that the sample was dominated by HAP (Fig. 3c). HPY peaks were less intense than in previous experiments, suggesting that less HPY formed.

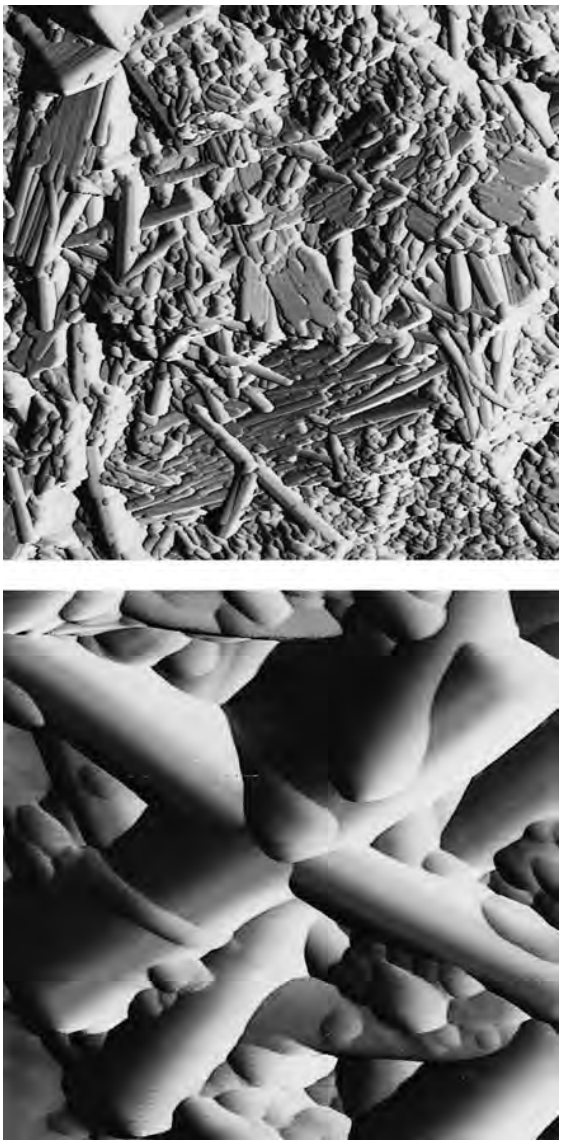

FIGURE 8. HAP reacted with 10 mg/L $[Pb_{aq}]_i$. (**top**) TMAFM image showing needles which appear to be preferentially oriented on another phase (scan area = 2.00 μm on a side). This is evidence in support of heterogeneous precipitation of HPY on the surface of HAP. (**bottom**) TMAFM image of an intergrowth with hexagonal symmetry (scan area = 700 nm on a side). SEM, TEM, EDS, and ED results (not shown) were similar to those at 100 mg/L $[Pb_{aq}]_i$. XRD pattern (see Fig. 3c) showed that the sample was dominated by HAP with lesser amounts of HPY.

1 and 0.5 mg/L $[Pb_{aq}]_i$

As is to be expected at such low concentrations of initial Pb_{aq}, many TMAFM images of the reaction product showed features consistent with the reaction blank. Numerous images of samples at an $[Pb_{aq}]_i$ of 1 mg/L also showed needle-shaped phases associated with the surface HAP, as well as needle-like phases that appeared to growing from HAP (Fig. 9). Several images at an $[Pb_{aq}]_i$ of 0.5 mg/L, revealed needle-like precipitates preferentially oriented on the surface of HAP (Fig. 10). These precipitates do not appear to be parallel intergrowths that formed in solution. The details of their association indicate heterogeneous precipitation of a solid Pb phase on the surface of HAP. We did not detect isolated HPY needles or clusters of needles without associated HAP. These results differed from those at higher $[Pb_{aq}]_i$ in that all of the needles appeared to be preferentially aligned on the surface of HAP or growing heterogeneously on HAP. TMAFM was

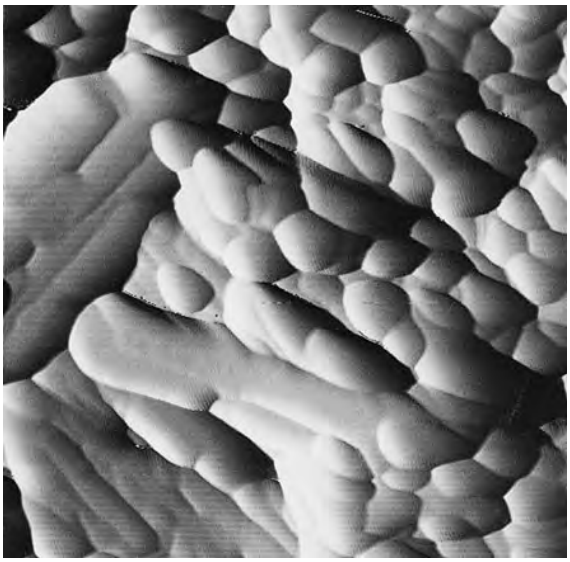

FIGURE 9. HAP reacted with 1 mg/L $[Pb_{aq}]_i$. TMAFM image showing a needle-like phase which appeared to be growing from another phase (scan area = 710 nm on a side). Based on XRD analysis, most of the material in the TMAFM images was HAP. All detectable Pb_{aq} was removed from solution and no such needle-like phases were detected in the reaction blank. Therefore, this is evidence of heterogeneous precipitation of a solid Pb phase. SEM, TEM, XRD, and EDS results (not shown) were similar to those of the reaction blank.

not capable of atomic resolution in air. Therefore our techniques did not allow us to rule out other Pb_{aq} sorption processes, such as adsorption, which may have occurred simultaneously. SEM and TEM revealed images that were indistinguishable from the HAP reaction blank. HAP was the only phase detected by XRD (Fig. 3b). HPY may have been present but at levels below the detection limit. Alternatively Pb_{aq} may have been adsorbed to HAP, or Pb_{aq} may have precipitated as an amorphous phase. EDS results were incapable of determining the distribution of Pb in the sample.

DISCUSSION

Macroscopic results showed the rapid removal of Pb_{aq} from solution. Direct methods, such as microscopy, spectroscopy, and diffraction allowed us to determine that the loss of Pb_{aq} from solution (i.e., sorption) was in large part because of the precipitation of a solid phase. The processes of sorption varied with the initial saturation state of the system at various $[Pb_{aq}]_i$.

Our observations of HPY needles at high concentrations of Pb_{aq} ($\geq$10 mg/L $[Pb_{aq}]_i$) support the hypothesis of Ma et al. (1993) that Pb_{aq} sorbs largely by the dissolution of HAP and subsequent formation of HPY according to the following equations:

$$Ca_5(PO_4)_3OH + 7H^+ \overset{\text{dis}}{\longleftrightarrow} 5Ca^{2+} + 3H_2PO_4^- + H_2O$$

$$5Pb^{2+} + 3H_2PO_4^- + H_2O \overset{\text{ppt}}{\longleftrightarrow} Pb_5(PO_4)_3OH + 7H^+.$$

At lower levels of $[Pb_{aq}]_i$ (<10 mg/L) it is unclear whether such a process takes place, however it is certain that a solid Pb phase precipitated on the surface of HAP.

Nucleation and growth of HPY

The saturation state of our systems with respect to HPY (Ω_{HPY}) is given by the following equation:

$$\Omega_{HPY} = \frac{[Pb^{+2}]^5[PO_4^{-3}]^3[OH^-]}{K_{sp}},$$

where $[i]$ represents the concentration (or more accurately the activity) of ion i in solution and K_{sp} is the equilibrium solubility product of HPY at a given temperature, pressure, and ionic strength. Reported values for the equilibrium solubility product of HPY differ by over 70 orders of magnitude. For example, one source cites a log K_{sp} value of -4.04 (Lindsay 1979), whereas another gives a value of -76.8 (Nriagu 1972). This discrepancy probably results partially from the difficulty in measuring solubility products for highly insoluble minerals such as HPY.

Our data only allow us to evaluate the initial saturation states of the experiments. These reactions have already been shown to be extremely rapid. Hence the initial saturation state is a very brief state of the system. Nevertheless, a qualitative measure of the initial saturation state provided an excellent means of comparing the driving forces for the sorption of Pb_{aq} under different experimental conditions.

Each experiment had the same initial conditions (temperature, pH, phosphate concentration, stirring rate) except for its $[Pb_{aq}]_i$; therefore, the $[Pb_{aq}]_i$ played an important role in determining the differences in initial saturation states. As such, the highest $[Pb_{aq}]_i$ in solution (500 mg/L) corresponded to the highest initial saturation state and vice versa.

Our complementary results allowed us to compare the observed morphology of Pb-precipitates to that predicted from nucleation and growth theory (Fig. 1b). At high saturation, homogeneous precipitation of numerous small nuclei are favored (e.g., Fig. 1b, $[Pb_{aq}]_i > 100$ mg/L). The product of HAP reacted with an $[Pb_{aq}]_i$ of 500 mg/L revealed the presence of many, very small aggregates and intergrown HPY needles (e.g., Fig. 6) that appear to have resulted from rapid precipitation of numerous small nuclei in solution. At intermediate saturation, fewer but more well-defined crystals are predicted to grow in solution (e.g., Fig. 1b, $[Pb_{aq}]_i$ = 100 mg/L). At $[Pb_{aq}]_i$ of 10–100 mg/L, microscopic images revealed larger, euhedral needles composed of relatively well developed prism and dipyramidal faces (e.g., Figs. 4b, 8b, and 8c). These needles appear to have resulted from dominating growth processes. Finally, at extremely low saturation, heterogeneous precipitation is favored (e.g., Fig. 1b, $[Pb_{aq}]_i < 10$ mg/L). With AFM, we observed this type of mechanism at $[Pb_{aq}]_i$ 10 mg/L (Figs. 8a, 9, and 10). We cannot be certain that HPY precipitated at such low $[Pb_{aq}]_i$. Heterogeneous growth of a Pb-phosphate phase on HAP may have crystallized as Pb-substituted HAP.

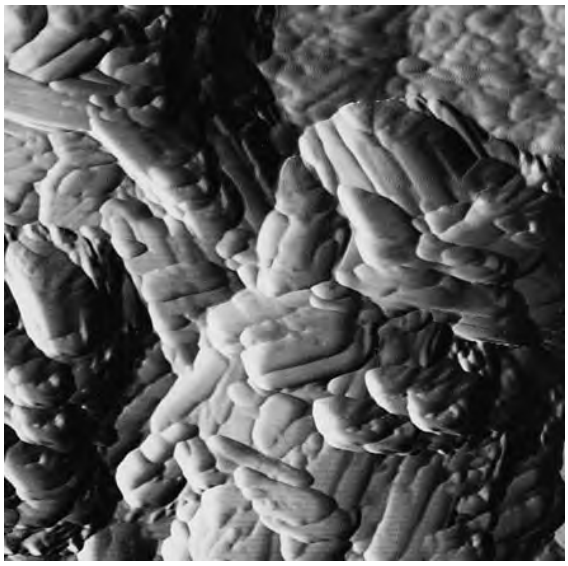

FIGURE 10. HAP reacted with 0.5 mg/L $[Pb_{aq}]_i$. TMAFM image showing a needle-like phase preferentially oriented on the surface of another phase (scan area = 1.60 μm on a side). Coupled with other results, this is evidence of heterogeneous nucleation of a solid Pb phase on the surface of HAP. SEM, TEM, XRD, and EDS results (not shown) were similar to those of the reaction blank.

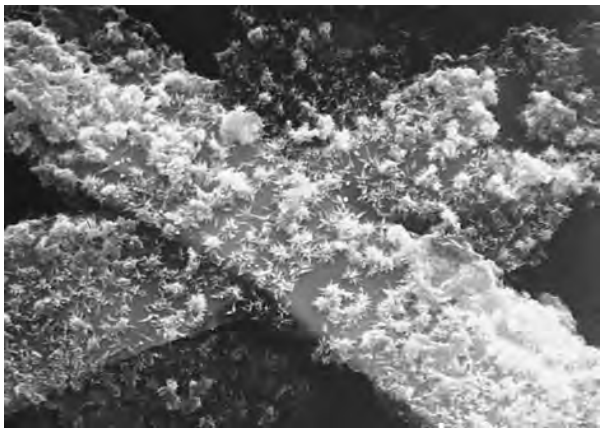

FIGURE 11. HAP reacted with 100 mg/L $[Pb_{aq}]_i$ and allowed to age for several days. SEM image of needles of HPY (image size = 23 × 16 μm). The needles of HPY grew significantly larger because of Ostwald ripening (compare with Fig. 8b); yet, some small needles remained as rosettes on the surface of these larger needles.

Sample aging effects

The experiment with an $[Pb_{aq}]_i$ of 100 mg/L was allowed to react for another five days, filtered and analyzed with TMAFM and SEM. TMAFM was unsuccessful because of tip-sample shape interaction as discussed above. SEM results showed much larger needles than those imaged after 2 h (e.g., length >25 μm and width >5 μm), and many had small rosettes on their surfaces (Fig. 11). EDS showed that these needles were dominated by Pb and P.

The needles of HPY appear to increase in size as they aged in solution, perhaps because of Ostwald ripening (Steefel and van Cappellen 1990). The small needles of HPY that precipitated after 2 h (e.g., Fig. 7b) had a larger surface area per unit volume relative to the aged needles, and therefore they may have been unstable. Apparently, the small HPY crystals were a precursor phase that underwent a transformation to a more stable morphology. Ostwald ripening generally occurs by the gradual increase in particle size, so that we cannot at present explain the bimodal particle size distribution (large needles vs. small rosettes). Although the smaller rosettes may have precipitated upon drying, this is unlikely given the drying procedure that we used.

In most cases HAP removes all detectable Pb_{aq} from solution in a matter of minutes to hours. Hence the system is in apparent macroscopic equilibrium with respect to Pb_{aq}. However these results indicate that although the system may have reached a macroscopic equilibrium, it had not achieved microscopic equilibrium. This result may have important implications for use of apatites to remediate Pb contaminated soils, in that the alternating wet and dry cycles of soil environments may influence the kinetics of the overall process.

Comparison of AFM, SEM, and TEM

This study benefited greatly from the complementary information provided by each form of microscopy. In general, we found that it was rewarding to apply all three techniques to the same sample to gain a better understanding of reaction processes. AFM provided higher resolution of surfaces and morphological details that promoted the comparison of microscopic images to macroscopic results in greater detail, especially at the lowest $[Pb_{aq}]_i$. SEM provided better images of larger needles (i.e., needles with lengths >2 μm), and TEM provided the best images of extremely small needles (i.e., needles with lengths <1 μm). Spectroscopic and diffraction capabilities of SEM and TEM facilitated identification and allowed determination of phase association in heterogeneous samples.

A major disadvantage of AFM was tip-sample shape interaction that commonly precluded imaging and sometimes distorted morphology (i.e., rounding of the ends of needles). This study demonstrated the importance of applying other forms of microscopy to validate AFM observations. Another disadvantage of AFM was that its analysis time was much longer than those for similar samples with SEM and TEM. Disadvantages of SEM and TEM lie in the destructive nature of these techniques. For example, samples are coated with carbon or gold. Furthermore, the electron beam can convert HAP to other Ca-phosphate phases during imaging (Huaxia and Marquis 1991).

Finally, AFM can be operated in ambient environmental conditions. Hence, the validation of AFM in air allows such a technique to be applied to a solution environment to ob-

serve reactions in real time. It is perhaps this final point that sets AFM apart from the other forms of microscopy.

Acknowledgments

This research benefited greatly from discussions with many colleagues, including: V. Laperche (Ohio State University), J. Hughes (Miami University), and M.F. Hochella Jr. and his research group at Virginia Polytechnic Institute and State University. M. Manecki (Kent State University) and R. Klouda (Liquid Crystal Institute) provided assistance with SEM; H. Colijn (Ohio State University) provided assistance with TEM and ED. Funding for S.K.L. was provided by the Water Resources Research Institute at Kent State University. S.K.L. also thanks J. Lower and T. Lower for their continued support and encouragement. Finally, we thank J. Rakovan (Virginia Polytechnic Institute and State University) and an anonymous reviewer for their helpful comments.

References cited

Barrón, V., Gálvez, N., Hochella, M.F. Jr., and Torrent, J. (1997) Epitaxial overgrowth of goethite on hematite synthesized in phosphate media: A scanning force and transmission electron microscopy study. American Mineralogist, 83, 1089–1098.

Benjamin, M.M. and Leckie, J.O. (1981) Multi-site adsorption of Cd, Co, Zn, and Pb on amorphous iron oxyhydroxide. Journal of Colloid and Interface Science, 79, 209–221.

Berner, R.A. (1978) Rate control of mineral dissolution under earth surface conditions. American Journal of Science, 278, 1235–1252.

———(1981) Kinetics of weathering and diagenesis. In Mineralogical Society of America Reviews in Mineralogy, 8, 111–134.

Davis, A., Ruby, M.V., and Bergstrom, P.D. (1992) Mineralogic controls on arsenic and lead bioavailability in soils from the Butte mining district, Montana, USA. Environmental Science and Technology, 26, 461–468.

Davis, A., Drexler, J.W., Ruby, M.V., and Nicholson, A. (1993) Micromineralogy of mine wastes in relation to lead bioavailability, Butte, Montana. Environmental Science and Technology, 27, 1415–1425.

Drever, J.I. (1988) The geochemistry of natural waters (2nd edition), 437 p. Prentice Hall, Englewood Cliffs, New Jersey.

Eggleston, C. (1994) High resolution scanning probe microscopy: Tip-surface interaction, artifacts, and applications in mineralogy and geochemistry. In A.E. Blum and K. Nagy, Eds., Scanning probe microscopy of clay minerals, p. 1–90. Clay Minerals Society, Boulder, Colorado.

Elliott, J.C. (1971) Monoclinic space group of hydroxyapatite. Nature Physical Science, 230, 72.

Elliott, J.C., Mackie, P.E., and Young, R.A. (1973) Monoclinic hydroxyapatite. Science, 180, 1055–1057.

Griffith, J.E. and Grigg, D.A. (1993) Dimensional metrology with scanning probe microscopes. Journal of Applied Physics, 74, R83–R109.

Hochella, M.F. Jr. (1990) Atomic structure, microtopography, composition, and reactivity of mineral surfaces. In Mineralogical Society of America Reviews in Mineralogy, 23, 87–132.

Huaxia, J. and Marquis, P.M. (1991) Modification of hydroxyapatite during transmission electron microscopy. Journal of Materials Science Letters, 10, 132–134.

Hughes, J.M., Cameron, M., and Crowley, D.K. (1989) Structural variations in natural F, OH, and Cl apatites. American Mineralogist, 74, 870–876.

———(1990) Crystal structures of natural ternary apatites: Solid solution in the $Ca_5(PO_4)_3X$ (X = F, OH, Cl) system. American Mineralogist, 75, 295–304.

Jackson, M.L. (1969) Soil chemical analysis-Advanced course (2nd edition), 845 p. Department of Soil Science, University of Madison, Wisconsin.

Junta, J.L. and Hochella, M.F. Jr. (1994) Manganese (II) oxidation at mineral surfaces: A microscopic and spectroscopic study. Geochimica et Cosmochimica Acta, 58, 4985–4999.

Kay, M.I., Young, R.A., and Posner, A.S. (1964) Crystal structure of hydroxyapatite. Nature, 204, 1050–1052.

Klein, C. and Hurlbut, C.S. Jr. (1985) Manual of mineralogy (20th edition), 596 p. Wiley, New York.

Lindsay, W.L. (1979) Chemical equilibria in soils, 449 p. Wiley, New York.

Lower, S.K. (1997) Pb sorption to hydroxylapatite: A microscopic, spectroscopic, and diffraction study, 170 p. M.S. thesis, Kent State University, Kent, Ohio.

Ma, Q.Y., Traina, S.J., Logan, T.J., and Ryan, J.A. (1993) In situ lead immobilization by apatite. Environmental Science and Technology, 27, 1803–1810.

Ma, Q.Y., Logan, T.J., Traina, S.J., and Ryan, J.A. (1994a) Effects of NO_3^-, Cl^-, F^-, SO_4^{2-}, and CO_3^{2-} on Pb^{2+} immobilization by hydroxyapatite. Environmental Science and Technology, 28, 408–418.

Ma, Q.Y., Traina, S.J., Logan, T.J., and Ryan, J.A. (1994b) Effects of aqueous Al, Cd, Cu, Fe(II), Ni, and Zn on Pb immobilization by hydroxyapatite. Environmental Science and Technology, 28, 1219–1228.

Ma, Q.Y., Logan, T.J., and Traina, S.J. (1995) Lead immobilization from aqueous solutions and contaminated soils using phosphate rocks. Environmental Science and Technology, 29, 1118–1126.

Maurice, P.A. and Lower, S.K. (1998) Using atomic force microscopy to study soil mineral reactions. Advances in Agronomy, in press.

Moore, D.M. and Reynolds, R.C. Jr. (1989) X-ray diffraction and identification and analysis of clay minerals, 332 p. Oxford University Press, New York.

Morris, M.C., McMurdie, H.F., Evans, E.H., Pavetzkin, B., Parker, H.S., Pyrros, N.P., and Hubbard, C.R. (1984) Standard X-ray diffraction powder patterns-section 20, 145 p. National Bureau of Standards, Washington, D.C.

Murphy, J. and Riley, J.P. (1962) A modified single solution method for the determination of phosphate in natural waters. Analytica Chimica Acta, 27, 31–36.

Nagy, K. and Blum, A.E. (1994) Scanning probe microscopy of clay minerals, 239 p. Clay Minerals Society, Boulder, Colorado.

Narasaraju, T.S.B., Singh, R.P., and Rao, V.L.N. (1972) A new method of preparation of solid solutions of calcium and lead hydroxylapatite. Journal of Inorganic and Nuclear Chemistry, 34, 2072–2074.

Nash, W.P. (1984) Phosphate minerals in terrestrial igneous and metamorphic rocks. In J.O. Nriagu and P.B. Moore, Eds., Phosphate minerals, p. 215–241. Springer, Berlin.

Nielsen, A.E. (1964) The kinetics of precipitation, 151 p. MacMillan, New York.

Nriagu, J.O. (1972) Lead orthophosphates: I. Solubility and hydrolysis of secondary lead orthophosphate. Inorganic Chemistry, 11, 2499–2503.

———(1973a) Lead orthophosphates: II. Stability of chloropyromorphite at 25° C. Geochimica et Cosmochimica Acta, 37, 367–377.

———(1973b) Lead orthophosphates: III. Stability of fluoropyromorphite and bromopyromorphite at 25° C. Geochimica et Cosmochimica Acta, 37, 1735–1743.

———(1984) Formation and stability of base metal phosphates in soils and sediments. In J.O. Nriagu and P.B. Moore, Eds., Phosphate minerals, p. 319–329. Springer, Berlin.

O'Day, P.A., Brown, G.E., and Parks, G.A. (1994) X-ray absorption spectroscopy of cobalt(II) multinuclear surface complexes and surface precipitates on kaolinite. Journal of Colloid and Interface Science, 165, 269–289.

Parks, G.A. (1990) Surface energy and adsorption at mineral-water interfaces: An introduction. In Mineralogical Society of America Reviews in Mineralogy, 23, 133–175.

Posner, A.S., Blumenthal, N.C., and Betts, F. (1984) Chemistry and structure of precipitated hydroxyapatites. In J.O. Nriagu and P.B. Moore, Eds., Phosphate minerals, p. 330–350. Springer, Berlin.

Ruby, M.V., Davis, A., Kempton, J.H., Drexler, J.W., and Bergstron, P.D. (1992) Lead bioavailability: Dissolution kinetics under simulated gastric conditions. Environmental Science and Technology, 26, 1242.

Ruby, M.V., Davis, A., and Nicholson, A. (1994) In situ formation of lead phosphates in soils as a method to immobilize lead. Environmental Science and Technology, 28, 646–654.

Scheidegger, A.M. and Sparks, D.L. (1996) Kinetics of formation and dissolution of nickel surface precipitates on pyrophyllite. Chemical Geology, 132, 157–164.

Schwertmann, U. and Cornell, R.M. (1991) Iron oxides in the laboratory, 132 p. Weinheim, New York.

Sposito, G. (1986) Distinguishing adsorption from surface precipitation. In J.A. Davis and K.F. Hayes, Eds., Geochemical processes at mineral surfaces, p. 217–228. American Chemical Society, Washington.

Steefel, C.I. and Van Cappellen, P. (1990) A new kinetic approach to modeling water-rock interaction: The role of nucleation, precursors, and Ostwald ripening. Geochimica et Cosmochimica Acta, 54, 2657–2677.

Stumm, W. and Morgan, J.J. (1981) Aquatic chemistry (2nd edition), 796 p. Wiley, New York.

Suzuki, T., Hatsushika, T., and Hayakawa, Y. (1981) Synthetic hydroxyapatites employed as inorganic cation exchangers. Journal of the Chemical Society Faraday Transactions I, 77, 1059–1062.

Suzuki, T., Hatsushika, T., Miyake, M. (1982) Synthetic hydroxyapatites as inorganic cation exchangers: 2. Journal of the Chemical Society Faraday Transactions I, 78, 3605–3611.

Suzuki, T., Ishigaki, K., Miyake, M. (1984) Synthetic hydroxyapatites as inorganic cation exchangers: 3. Exchange characteristics of lead ions (Pb^{2+}). Journal of the Chemical Society Faraday Transactions I, 80, 3157–3165.

Takeuchi, Y. and Arai, H. (1990) Removal of coexisting Pb^{2+}, Cu^{2+} and Cd^{2+} ions from water by addition of hydroxyapatite powder, 3. pH and sample conditioning effects. Journal of Chemical Engineering of Japan, 23, 75–80.

Takeuchi, Y., Suzuki, T., and Arai, H.J. (1988) A study of equilibrium and mass transfer in processes for removal of heavy-metal ions by hydroxyapatite. Journal of Chemical Engineering of Japan, 21, 98–100.

Tiselius, A., Hjerten, S., and Levin, O. (1956) Protein chromatography on calcium phosphate columns. Archives of Biochemistry and Biophysics, 65, 132–155.

Xu, Y. and Schwartz, F.W. (1994) Lead immobilization by hydroxyapatite in aqueous solutions. Journal of Contaminant Hydrology, 15, 187–206.

Zhong, Q., Inniss, D., Kjoller, K., and Elings, V.B. (1993) Fractured polymer/silica fiber surface studied by tapping mode atomic force microscopy. Surface Science Letters, 290, L688–L692.

Manuscript received April 14, 1997
Manuscript accepted September 5, 1997